Morphology of the petrosal and stapes of Borealestes (Mammaliaformes, Docodonta) from the Middle Jurassic of Skye, Scotland

[Papers in Palaeontology, 2018, pp. 1–18]

MORPHOLOGY OF THE PETROSAL AND STAPES OF *BOREALESTES* (MAMMALIAFORMES, DOCODONTA) FROM THE MIDDLE JURASSIC OF SKYE, SCOTLAND

by ELSA PANCIROLI[1,2], JULIA A. SCHULTZ[3,4] *and* ZHE-XI LUO[3]

[1]School of Geosciences, Grant Institute, University of Edinburgh, Kings Buildings, Edinburgh, EH9 3FE, UK; elsa.panciroli@ed.ac.uk
[2]Natural Sciences Department, National Museums Scotland, Chambers St, Edinburgh, EH1 1JF, UK
[3]Department of Organismal Biology & Anatomy, University of Chicago, 1027 East 57th Street, Chicago, IL USA; zxluo@uchicago.edu
[4]Steinmann-Institut für Geologie, Mineralogie und Paläontologie, Universität Bonn, Nussallee 8, 53115, Bonn, Germany; jaschultzing@gmail.com

Typescript received 19 October 2017; accepted in revised form 1 May 2018

Abstract: We describe, in unprecedented detail, the petrosals and stapes of the docodont *Borealestes* from the Middle Jurassic of Scotland, using high resolution μCT and phase-contrast synchrotron imaging. We describe the inner ear endocast and the vascularized interior structure of the petrosal, and provide the first endocranial view of a docodontan petrosal. Our study confirms some similarities in petrosal and stapedial morphology with the better known *Haldanodon* of the Late Jurassic of Portugal, including: (1) the degree of curvature of the cochlea; (2) multiple features related to the highly pneumatized paroccipital region; (3) the shape of lateral trough, the fossa of the M. tensor tympani, and the ridge on the promontorium; (4) the round shape of the fenestra vestibuli; and (5) overall morphology of the stapes. But *Borealestes* differs from *Haldanodon* in having a bony ridge that separates the tympanic opening of the prootic canal, the secondary facial foramen and the hiatus Fallopii, from the fenestra vestibuli. We identify two new vascular structures: the anterior and posterior trans-cochlear sinuses, which traverse the pars cochlearis around the cochlear nerve (VIII). These trans-cochlear sinuses have not been observed in previous docodont specimens, and could be an autapomorphy of *Borealestes*, or apomorphic for this clade. We also establish the anatomical relationship of the circum-promontorium plexus to the inner endocast. The high quality of our scans has made these structures visible for the first time.

Key words: *Borealestes*, Mammaliaformes, docodont, petrosal, inner ear, endocast.

DOCODONTA comprise an extinct branch of Mammaliaformes that falls outside crown Mammalia, but are closer to crown mammals than *Sinoconodon*, morganucodontans, haramiyidans and kuehneotheriids (Wible & Hopson 1993; Luo *et al.* 2002; Kielan-Jaworowska *et al.* 2004; Martin 2005; Luo *et al.* 2015*a*). Docodonts retain the plesiomorphic association of the postdentary middle ear elements with the dentary in the postdentary trough (Lillegraven & Krusat 1991; Kielan-Jaworowska *et al.* 2004; Ji *et al.* 2006; Meng *et al.* 2015). Docodonts also possess complex cusps and crests on their molars, creating shearing and crushing surfaces, providing many characters that distinguish them from most contemporaneous stem mammaliaform families (Averianov & Lopatin 2006; Luo & Martin 2007; Luo *et al.* 2015*b*). Their derived molar morphology (Kermack *et al.* 1987; Sigogneau-Russell 2003; Meng *et al.* 2015; Schultz *et al.* 2017*a*) and very distinctive differences in postcranial skeletons are likely to have contributed to their wide ecological diversity during the Jurassic (Ji *et al.* 2006; Luo 2007; Meng *et al.* 2015).

Recent analyses suggest that docodonts may be closely related to *Woutersia* and *Delsatia* among the stem mammaliaforms of the Late Triassic (Sigogneau-Russell & Hahn 1995; Averianov & Lopatin 2006; Luo & Martin 2007). It was further proposed that docodonts may form a clade with *Tikitherium* (Datta 2005), to the exclusion of other Late Triassic mammaliaforms (Luo & Martin 2007).

Members of Docodonta are found in the Middle Jurassic Bathonian of the UK and Russia (Waldman & Savage 1972; Lopatin & Averianov 2005), and from equivalent stratigraphic levels elsewhere in Eurasia (Ji *et al.* 2006). During the Late Jurassic, their distribution further expanded to North America, encompassing the entire Laurasian landmass (Simpson 1929; Krusat 1980; Pfretzschner *et al.* 2005; Hu *et al.* 2007; Martin *et al.* 2010; Rougier *et al.* 2015; Luo *et al.* 2015*b*). One taxon extended to the Early Cretaceous of Russia (Maschenko *et al.* 2002; Lopatin *et al.* 2009). The taxon *Gondtherium* from Toarcian sediments in India, was suggested to be docodontan. This would increase the geographical range of this group (Prasad & Manhas 2001

doi: 10.1002/spp2.1233

2007). However, the docodont affinity of *Gondtherium* has been challenged (Averianov *et al.* 2010).

There were previously five docodonts for which reasonably complete cranial material is known: *Docodon*, *Haldanodon*, *Castorocauda*, *Agilodocodon* and *Docofossor*. Only the petrosal of *Haldanodon* has been recovered and described so far (Lillegraven & Krusat 1991; Ruf *et al.* 2013). Here we describe the petrosals of *Borealestes*, expanding the information on the cranial morphology of docodonts.

Borealestes is the oldest docodont for which cranial material is known, and can thus shed light on the comparative morphology of the petrosal of docodonts as a whole. We used high-resolution micro-computed tomography (μCT) and digital reconstruction to explore the petrosal anatomy, and to generate an endocast of the inner ear of *Borealestes*. We compare these with the petrosal and inner ear of *Haldanodon*, and other key Mesozoic mammals for which the petrosals are known. This comparison provides important new information on the characteristics of the inner ear of a primitive docodont, and the evolutionary transformation from the simpler inner ear in early mammals in general (Luo *et al.* 1995), to the complex inner ear morphology (including coiled cochlea) of stem therians and crown Theria (Luo 2001; Ruf *et al.* 2009, 2013; Luo *et al.* 2011; Luo *et al.* 2016; Schultz *et al.* 2017*b*).

GEOLOGICAL SETTING

The left petrosal of *Borealestes*, specimen NMS G.1992.47.121.2 is in the collections at the National Museum of Scotland (NMS) in Edinburgh, Scotland. It is part of the skeleton of *Borealestes* NMS G.1992.47.121.1 (which includes the right petrosal) recovered in 1972 by M. Waldman and R. J. G. Savage from the Jurassic limestone beds near Elgol, Isle of Skye. The exact location where the skeleton was recovered is yet to be determined (currently under investigation by EP), but the Kilmaluag comprises dolomitized blue–grey limestones, interbedded with calcareous siltstones and shales. Freshwater gastropods, bivalves, and ostracods (*Viviparus*, *Neomidon*, *Unio*, *Darwinula* and *Theriosynoecum*) indicate a freshwater, lagoonal environment (Andrews 1985; British Geological Survey 2011). The skeleton is believed to have come from 'the vertebrate beds', the strata that have yielded fossil lizards, crocodylomorphs, archosaurs, tritylodontids and mammals (Waldman & Savage 1972; Evans *et al.* 2005; Close *et al.* 2016; Panciroli *et al.* 2017*a*, *b*).

MATERIAL AND METHOD

NMS G.1992.47.121.1 is a fragmentary skeleton to which the left petrosal NMS G.1992.47.121.2 belongs, but from which it is now detached. The right petrosal is still part of the rock block of NMS G.1992.47.121.1. The skeleton has not yet been described, and is not identified to species level, but we confirm it belongs to the genus *Borealestes* (EP & Z-XL, pers. obs.; currently under study by EP). The left petrosal, along with several other bone fragments, was dislodged from the complete skeleton historically during handling, allowing them to be scanned and described separately. The right petrosal remained *in situ* with the skeleton. Micro-computed tomographic data (μCT) of NMS G.1992.47.121.2 were obtained using the μCT scanner built in-house at the University of Edinburgh, School of Geosciences Experimental Geoscience Facility. The scanner comprises a Feinfocus 10–160 kV dual transmission/reflection source, MICOS UPR-160-AIR ultra-high precision air-bearing table, Perkin Elmer XRD0822 amorphous silicon x-ray flat panel detector and terbium doped gadolinium oxy-sulfide scintillator. The scan resolution is 8.9 μm. Data acquisition software was written in-house, and scans were reconstructed using Octopus 8.7 software (https://octopusimaging.eu/). Phase-contrast synchrotron data from NMS G.1992.47.121.1 were obtained at the European Synchrotron Radiation Facility (ESRF), Grenoble, France. This produced data with a scan resolution of 6.15 μm, which was subsequently resampled to 12.3 μm.

These data were then digitally reconstructed and image processed using Mimics 19.0 at the National Museum of Scotland (https://www.materialise.com/en/medical/software/mimics). Digital reconstructions are available in the Dryad Digital Repository (Panciroli *et al.* 2018). Raw data are part of a dataset comprising the fragmentary skeleton NMS G.1992.47.121.1, currently under study by EP. The complete raw dataset will be available upon completion of this work and subsequent publication.

Institutional abbreviation. NMS, National Museums Scotland, Edinburgh, UK.

RESULTS

Petrosals

NMS G.1992.47.121.2 (Figs 1B–E, 2) is the separated left petrosal of *Borealestes*. The lateral trough, the mastoid region and the associated structures are not preserved in this petrosal. The pars cochlearis is also incomplete, missing the anteromedial portion (Figs 1D–E, 2F). Nonetheless, the promontorium, or ventral eminence of the pars cochlearis, is relatively well preserved and shows many surface features (Fig. 2C–E). The right petrosal (Figs 1F–G, 3–6) is considerably better preserved in the lateral trough, the cavum epiptericum, the prootic groove

structure, and in the paroccipital and mastoid regions. All of these structures are consistent with those identified in the petrosals of the docodont *Haldanodon* (Ruf *et al.* 2013). In the following, we describe each of the petrosal structures by referring to both petrosals.

A bony ridge is visible on the anterolateral aspect of the promontorium (Figs 2E, 5A). This promontorium ridge is better preserved on the right petrosal than the left. The main part of the promontorium bulges anteromedially and ventrally, best shown in the left petrosal (Fig. 2). On the right petrosal, a piece of promontorium is broken but has been digitally restored (Fig. 5). The bone is better preserved in the apical region of the pars cochlearis of the right petrosal (Fig. 5). However, an area of the endocranial surface is missing on the internal surface of the anterior pars cochlearis of the right petrosal.

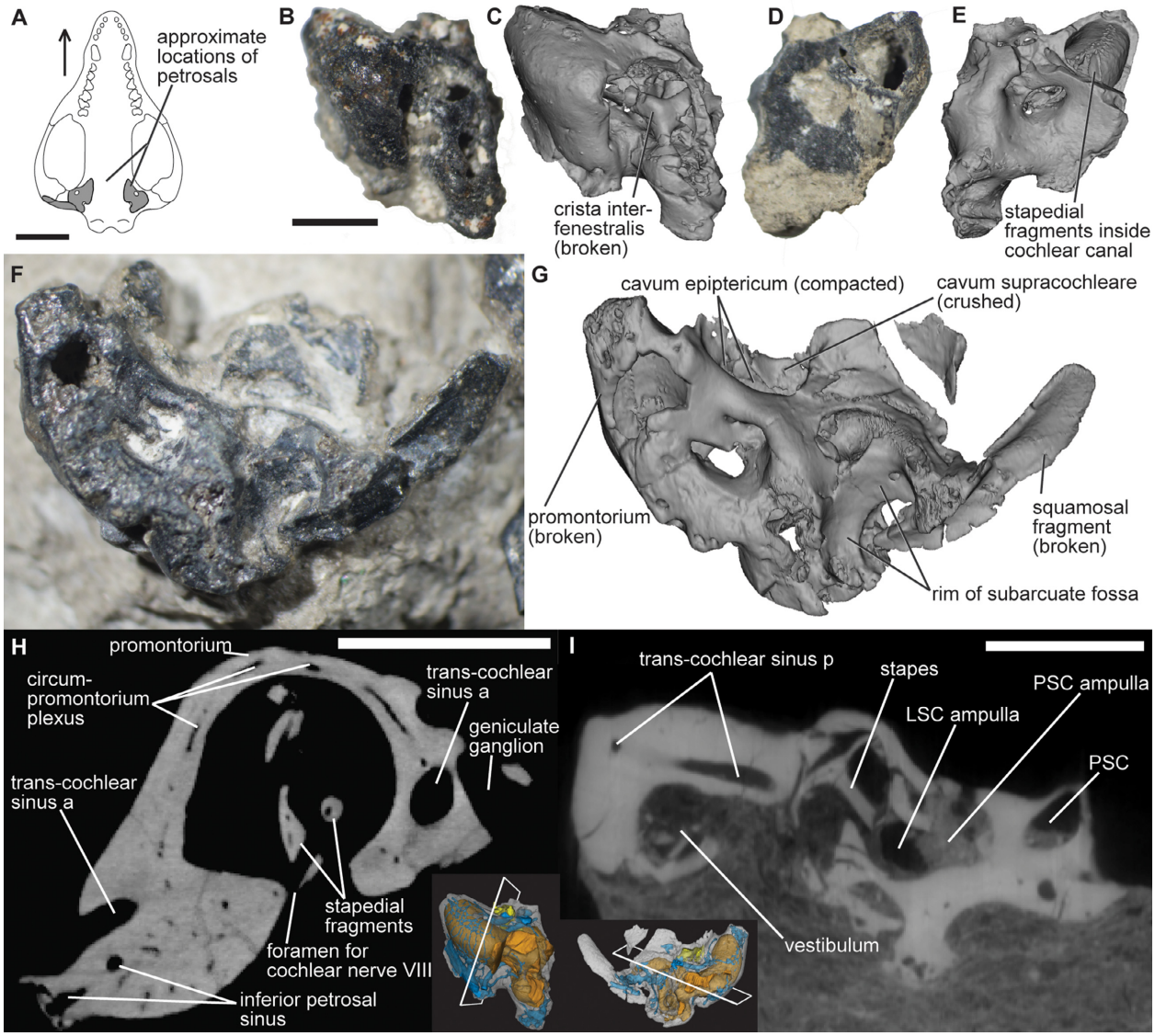

FIG. 1. Petrosals of the docodont *Borealestes*. Photos and digital reconstructions from μCT and synchrotron scans. A, approximate positions of preserved petrosals in schematic skull outline of docodont (simplified from *Haldanodon*, partly based on Ruf *et al.* 2013). B–E, left petrosal NMS G.1992.47.121.2: B, photo of left petrosal in ventral view; C, digital reconstruction in ventral view showing crushing and dislocated fragments inside petrosal; D, photo of left petrosal in endocranial view; E, digital reconstruction of the endocranial view showing fragments inside petrosal. F–G, right petrosal NMS G.1992.47.121.1: F, photo of right petrosal in endocranial view; G, digital reconstruction of right petrosal in endocranial view with main features labelled for orientation. H–I, μCT-scan slices with main features labelled and approximate position of slice picture shown in inset: H, left petrosal NMS G.1992.47.121.2; I, right petrosal NMS G.1992.47.121.1. *Abbreviations*: a, anterior; LSC, lateral semi-circular canal; p, posterior; PSC, posterior semi-circular canal. Scale bar in 1A represents 5 mm, all other scale bars represent 1 mm (scale bar in B also refers to C–G).

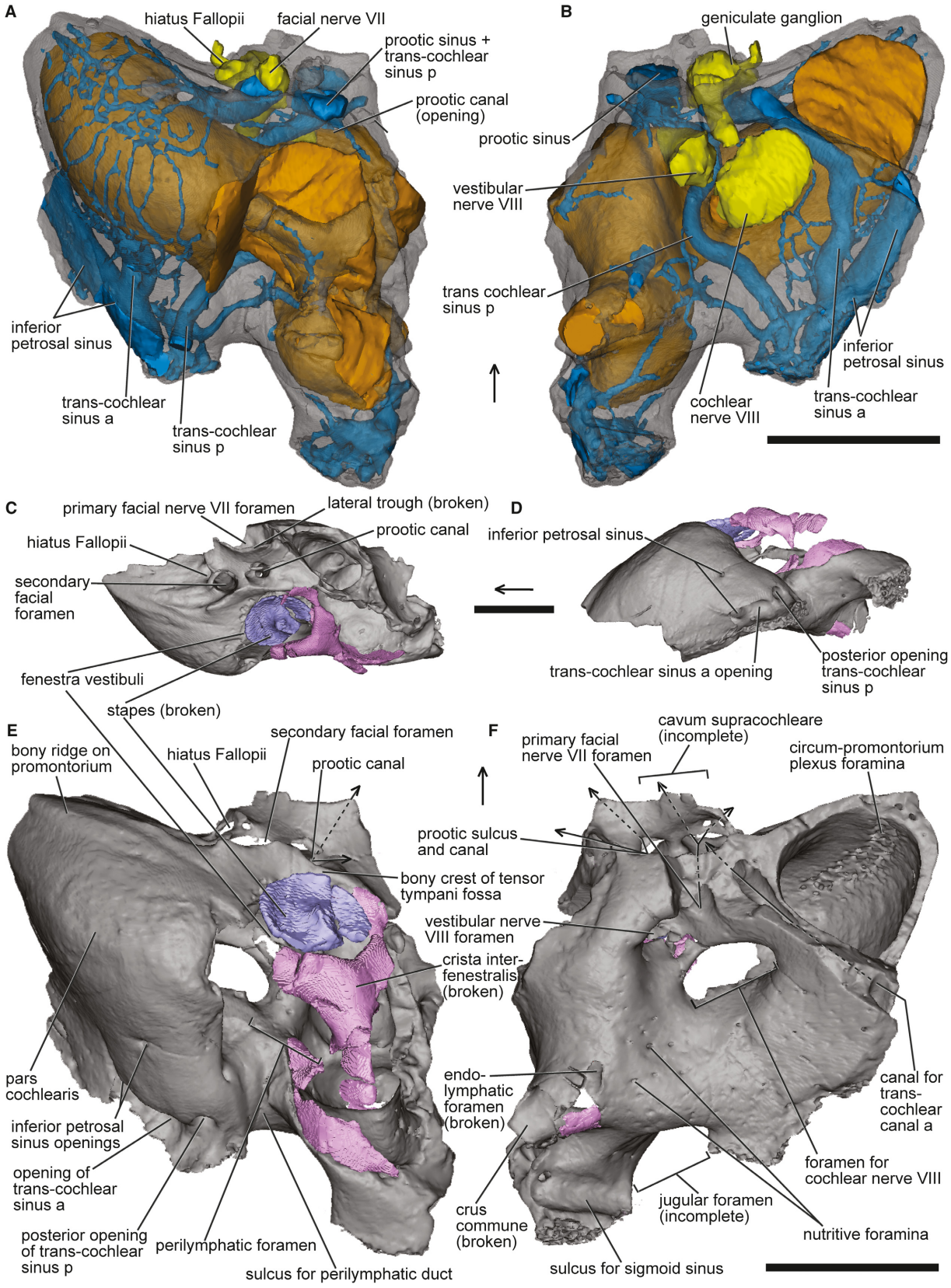
A
hiatus Fallopii
facial nerve VII
prootic sinus + trans-cochlear sinus p
prootic canal (opening)
inferior petrosal sinus
trans-cochlear sinus a
trans-cochlear sinus p
B
geniculate ganglion
prootic sinus
vestibular nerve VIII
trans cochlear sinus p
inferior petrosal sinus
cochlear nerve VIII
trans-cochlear sinus a
C
primary facial nerve VII foramen
lateral trough (broken)
prootic canal
hiatus Fallopii
secondary facial foramen
fenestra vestibuli
stapes (broken)
D
inferior petrosal sinus
trans-cochlear sinus a opening
posterior opening trans-cochlear sinus p
E
bony ridge on promontorium
hiatus Fallopii
secondary facial foramen
prootic canal
bony crest of tensor tympani fossa
vestibular nerve VIII foramen
crista inter-fenestralis (broken)
pars cochlearis
inferior petrosal sinus openings
opening of trans-cochlear sinus a
posterior opening of trans-cochlear sinus p
perilymphatic foramen
sulcus for perilymphatic duct
F
primary facial nerve VII foramen
cavum supracochleare (incomplete)
circum-promontorium plexus foramina
prootic sulcus and canal
endo-lymphatic foramen (broken)
canal for trans-cochlear canal a
foramen for cochlear nerve VIII
jugular foramen (incomplete)
crus commune (broken)
nutritive foramina
sulcus for sigmoid sinus

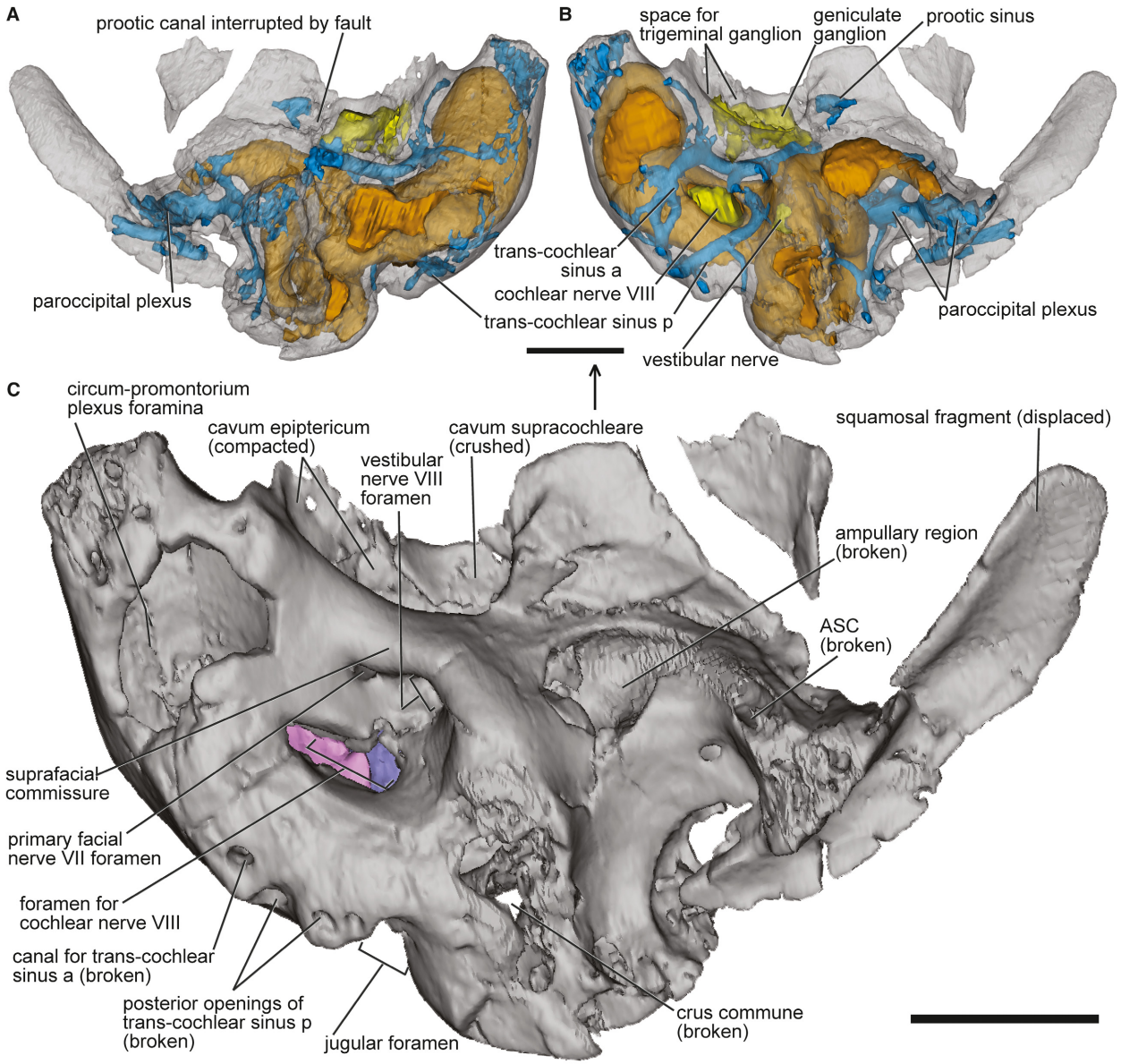

FIG. 3. Right petrosal of the docodont *Borealestes* NMS G.1992.47.121.1. Digital reconstructions from synchrotron scan. A–B, semi-translucent views of interior structures of the right petrosal in: A, ventral; B, endocranial view; blue = vascular structures; yellow = nerves; brown = inner ear endocast. C, major exterior structures preserved on the endocranial aspect of the right petrosal. More detailed identification shown in stereo paired images in Figure 4. Arrows indicates anterior direction. *Abbreviations*: a, anterior; p, posterior. Scale bars represent 1 mm.

The entire apical region is broken off on the left (Fig. 2). These breakages help to expose the tiny foramina of the circum-promontorium plexus on the interior surface of the cochlear canal (Figs 2F, 3C).

The crista interfenestralis is present, separating the fenestra vestibuli from the perilymphatic foramen and connecting the promontorium with the more posteriorly located mastoid region in complete petrosals, as in other

FIG. 2. Left petrosal of the docodont *Borealestes* NMS G.1992.47.121.2. Digital reconstructions from µCT scan. A–B, semi-translucent views of interior structures of the left petrosal in: A, ventral; B, endocranial view; blue = vascular structures; yellow = nerves; brown = inner ear endocast. C–F, exterior surface structure with repositioned stapes (lilac), and periphery of fenestra vestibuli and crista interfenestralis (pink): C, dorso-lateral view (tilted); D, medial view (tilted); E, ventral (external) view; F, dorsal (endocranial) view. Arrows indicate anterior direction. *Abbreviations*: a, anterior; p, posterior. All scale bars represent 1 mm.

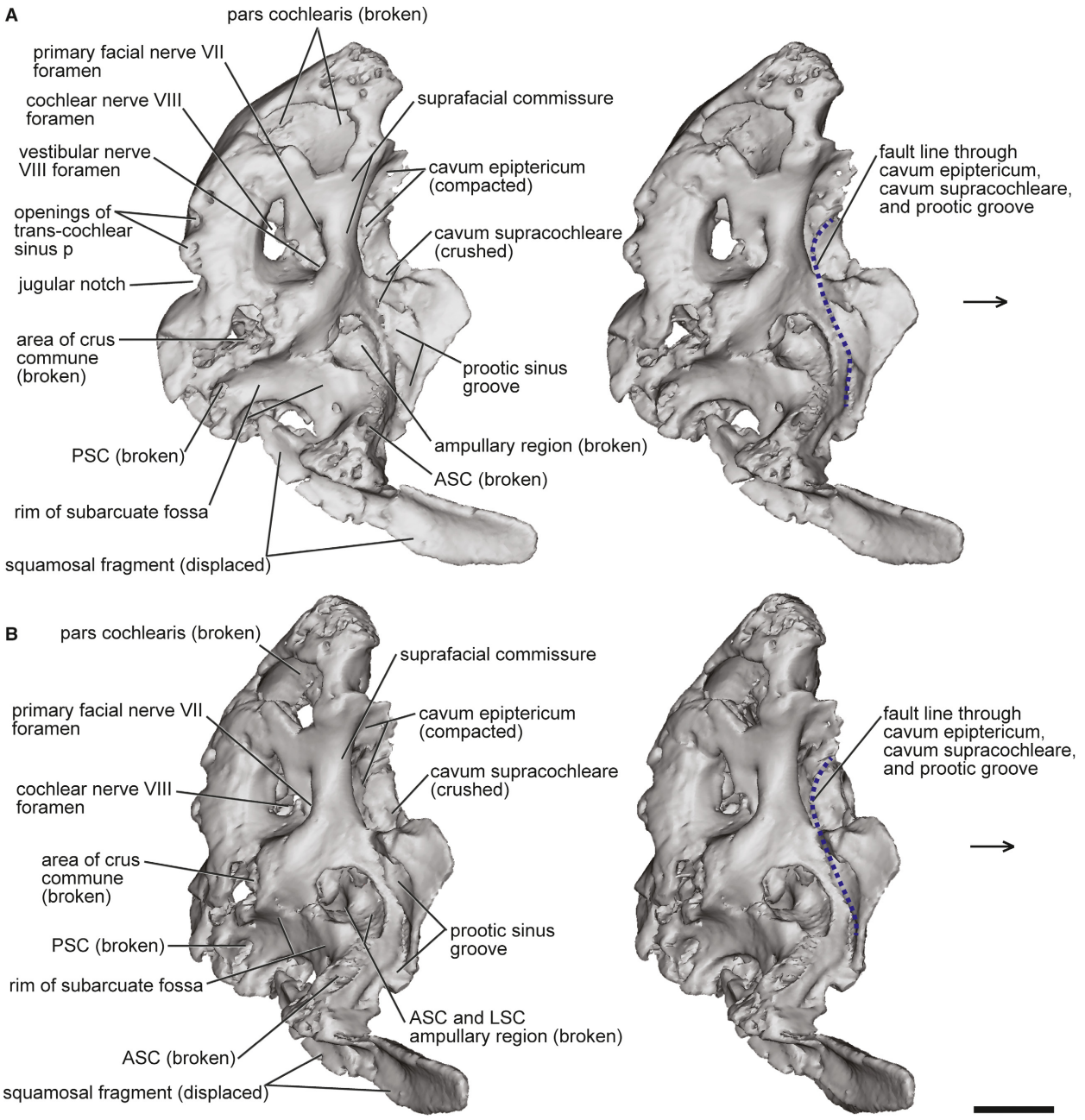

FIG. 4. Stereo pairs of right petrosal of the docodont *Borealestes* NMS G.1992.47.121.1. Endocranial view from digital reconstructions of synchrotron scans. Exterior structures preserved on the endocranial (internal) aspect of the right petrosal. A, dorsal view (stereo pair). B, dorsolateral view (stereo pair). The petrosal has a major fracture (fault) indicated by dashed-line that cuts through the bone, along the prootic sinus groove, and then the cavum supracochleare that contained the geniculate ganglion. Further anteriorly, distortion by the same fault compacted the cavum epiptericum for the trigeminal ganglion, compressing this structure into a narrow space. Arrows indicate anterior direction. *Abbreviations*: ASC, anterior semi-circular canal; LSC, lateral semi-circular canal; p, posterior; PSC, posterior semi-circular canal. Scale bar represents 1 mm. Colour online.

Mesozoic mammals (Rougier *et al.* 1996; Ruf *et al.* 2009, 2013; Luo *et al.* 2012). The crista interfenestralis is intact in the right petrosal (Figs 5A, 6), but on the left petrosal (Fig. 2) it is fractured and collapsed into the hollowed inner ear space of the petrosal. Despite this, it can still be recognized without question, and has been digitally restored to its original position (Fig. 2C–F).

The left petrosal shows several posterior openings of the inferior petrosal sinus canal, anteromedial to the perilymphatic sulcus (and also anterior to the jugular notch)

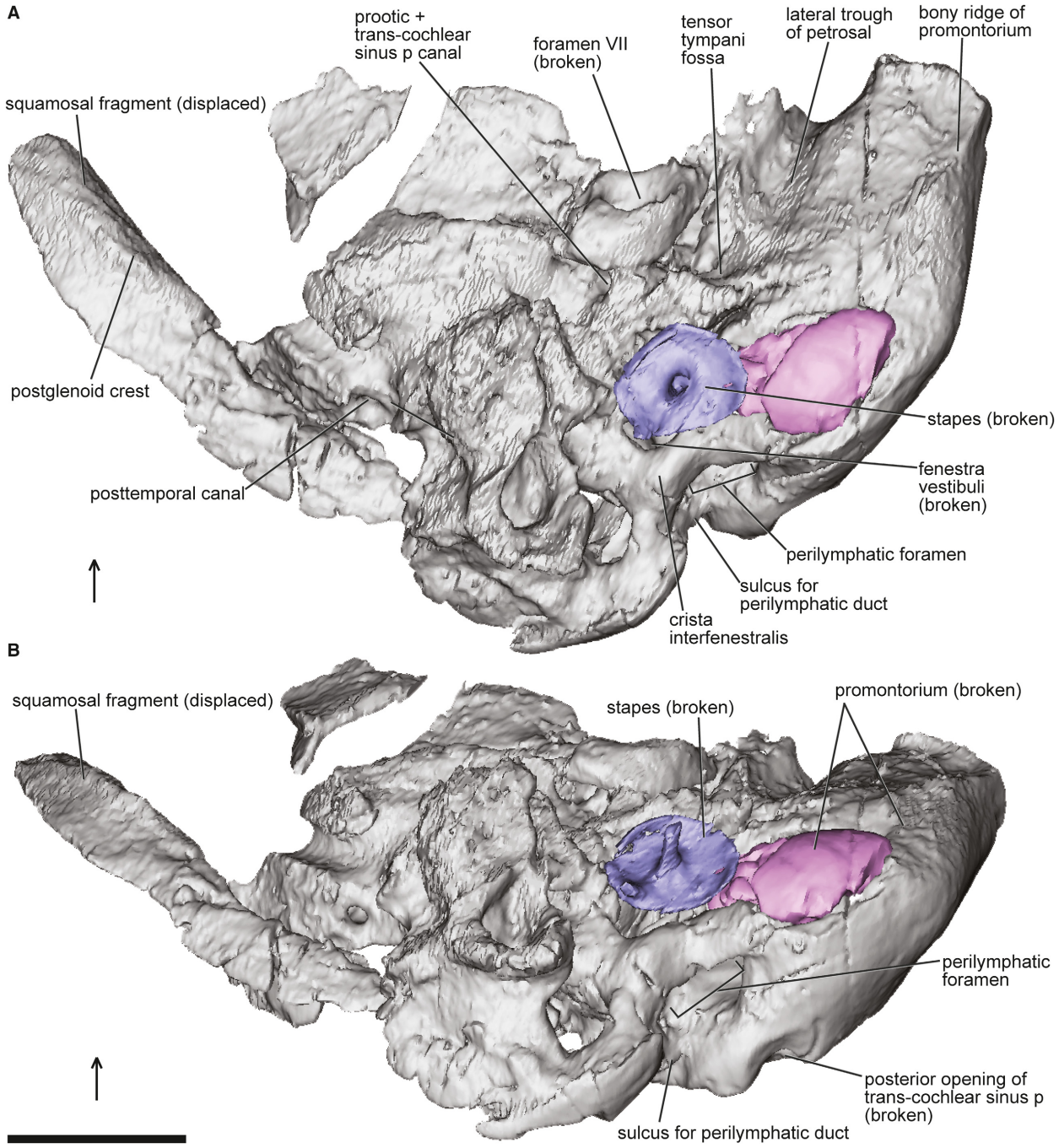

FIG. 5. Right petrosal of the docodont *Borealestes* NMS G.1992.47.121.1. Digital reconstructions of ventral view from synchrotron scan. External surface structures with the stapes restored to the fenestra vestibuli, and displaced promonotium fragments repositioned. A, ventrolateral view; B, ventromedial view. For full structural identifications see Figure 6. The petrosal is associated with a broken and displaced strip of the squamosal. Arrows indicate anterior direction. *Abbreviation*: p, posterior. Scale bars represent 1 mm. Colour online.

on the posteromedial corner of the promontorium (Fig. 2). Of these, the first opening is large, and anteromedially located. This opening is connected to the inferior petrosal sinus, enclosed in a thick bony canal along the medial edge of the pars cochlearis. This is termed the opening of the inferior petrosal sinus. A second, smaller opening is located lateral to the first opening, and this tiny foramen is also connected to a small tributary channel networked with the inferior petrosal sinus (Fig. 2). These surface foramina can be traced to the inferior

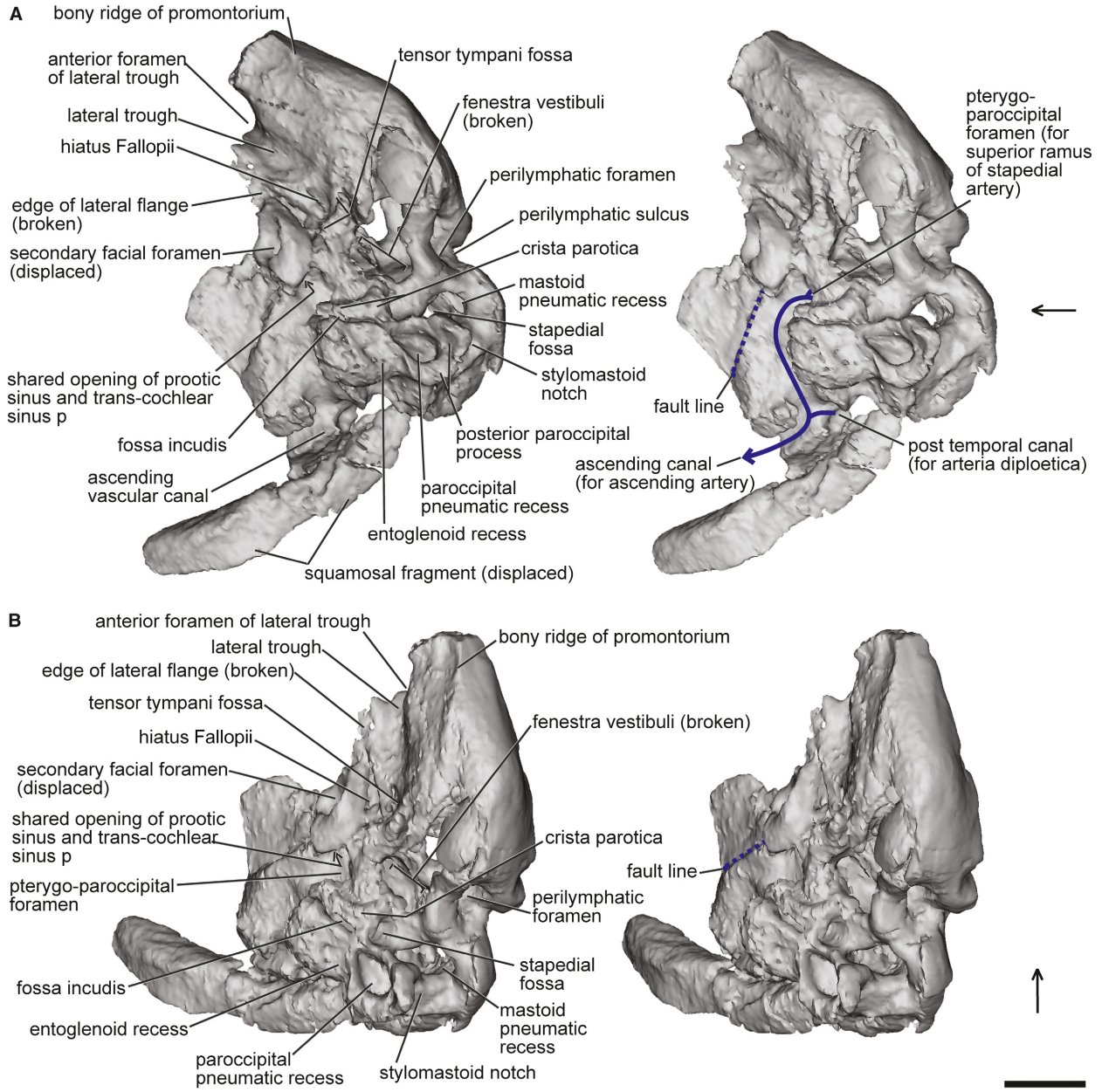

FIG. 6. Stereo pairs of the right petrosal of the docodont *Borealestes* NMS G.1992.47.121.1. Ventral view from digital reconstructions from synchrotron scans. Exterior structures preserved on the ventral aspect of the right petrosal. A, ventrolateral view (stereo pair); B, ventral view (stereo pair). The petrosal has a major fracture (fault) indicated by dashed-line that cuts through the bone along the prootic groove and its canal, and then through the cavum supracochleare that contained the geniculate ganglion. This has distorted the cavum supracochleare and dislocated the opening of the secondary facial foramen. Further anteriorly the same fault compacted the cavum epiptericum for the trigeminal ganglion, and compressed this structure. The lateral flange of the petrosal is broken, and only shown in its remaining and broken edge. The associated and incomplete strip of squamosal is displaced. A piece of petrosal anterior lamina, and the broken piece of the promontorium are omitted from these renderings. The solid lines with arrows indicate the interpreted courses of superior ramus of stapedial artery (via pterygo-paroccipital foramen), the arteria diploetica magna (via the post-temporal canal) and the ascending vessel of temporal region from the confluence of these two vessels. Arrows indicate anterior direction. *Abbreviation*: p, posterior. Scale bar represents 1 mm. Colour online.

petrosal sinus in the medial (or inferior) part of pars cochlearis, as in the petrosals of the docodont *Haldanodon* and other Mesozoic mammals (Wible 1990; Rougier *et al.* 1992, 1996; Ladevèze & de Muizon 2007, 2010; Luo *et al.* 2012; Ruf *et al.* 2013). The bony canal of the large inferior petrosal sinus is only preserved partially on the

left petrosal, and both its anterior part (near the apex of pars cochlearis) and its posterior section are broken (Fig. 2). The broken posterior part of the inferior petrosal sinus canal is connected to a trans-cochlear sinus channel (described below). Of the three openings connected to inferior petrosal sinus, the posterior-most opening is also the opening of the posterior trans-cochlear sinus. The interpretation of how the inferior petrosal sinus is connected to the trans-cochlear sinus channel is based on the left petrosal, as the medial edge of the pars cochlearis where the inferior petrosal sinus would be located has been eroded in the right petrosal.

In both the left and right petrosals, we have visualized and identified two vascular channels that traverse the pars cochlearis through the bone, respectively called the anterior trans-cochlear sinus, and the posterior trans-cochlear sinus (Figs 2, 3, 7). The anterior trans-cochlear sinus channel is confluent with the posterior end of the inferior petrosal sinus (Figs 2A, B), but the posterior trans-cochlear sinus has its own opening on the posteromedial corner of the promontorium (Figs 2A, D–E). In the right petrosal, because the media edge containing the canal of the inferior petrosal sinus has been eroded and lost, the two openings of the anterior trans-cochlear sinus and the posterior trans-cochlear sinus appear well separated (Fig. 3).

The bony floor of the lateral trough is only partly preserved in the left petrosal (NMS G.1992.47.121.2) but is more complete in the right petrosal (NMS G.1992.47.121.1). The lateral flange is preserved as a broken edge on the right petrosal, and is altogether lost in the left petrosal (Figs 2, 5, 6). The following structures can be identified in the posterior part of lateral trough: the hiatus Fallopii for the greater petrosal nerve; the secondary facial nerve foramen (on the lateral wall of cavum supracochleare); and a large opening for the confluent prootic canal and the tympanic opening of the posterior trans-cochlear sinus channel (Figs 2, 3). We also interpret a shallow depression area anterior to the fenestra vestibule, and near the opening of the hiatus Fallopii, as the fossa for the tensor tympani along the posterior rim of the lateral trough. The depression we have interpreted as the tensor tympani fossa is similar in location to the tensor tympani fossa identified in the petrosals of Cretaceous multituberculates, and in the Cretaceous triconodontid from the Cloverly Formation (Wible & Hopson 1993, fig. 5.3; see also Wible & Hopson 1995, figs 7, 8). Posteromedially, a bony ridge separates the prootic canal, secondary facial foramen and hiatus Fallopii from the fenestra vestibuli, forming part of the latter's anterior rim. The secondary facial foramen is anterior to the prootic canal opening.

The crista interfenestralis is crushed and displaced dorsally in the left petrosal NMS G.1992.47.121.2, distorting the original shape and proportions of the fenestra vestibuli and the perilymphatic foramen (Figs 1C, 2E). Although the crista interfenestralis is better preserved in the right petrosal, the promontorial roof in this region is broken. The lateral periphery of the fenestra vestibuli is also broken. The preservational defects have distorted the shape of the fenestra vestibuli. The preserved shape of stapedial foot plate (described below) can give a reliable approximation to the shape of the fenestra vestibuli. We digitally repositioned the fragments of the crista interfenestralis of specimen NMS G.1992.47.121.2, to partially restore the periphery of the fenestra vestibuli. Based on the restoration, we interpret the fenestra vestibuli as being more or less round in circumference, as reflected in the shape of the stapedial footplate (Figs 2, 5, 8). Both the fenestra vestibuli and the perilymphatic foramen are large, relative to the size of the promontorium. The fenestra vestibuli is positioned posterolaterally to the promontorium, and the perilymphatic foramen is posterior to the promontorium.

A perilymphatic sulcus for the perilymphatic duct (aquaeductus cochleae) is present in both petrosals. This sulcus connects the perilymphatic foramen and the margin of the jugular foramen (Figs 2E, 5, 6). This is similar to other stem mammals and several Mesozoic clades of crown mammals (Kermack *et al.* 1981; Crompton & Luo 1993; Wible & Hopson 1993; Lillegraven & Hahn 1993; Wible & Hopson 1995; Rougier *et al.* 1996; Luo *et al.* 2001). The jugular foramen is only represented by its margin on the petrosal; the medial periphery of this foramen is not preserved in this specimen.

In the endocranial aspect of the digital reconstruction, the osseous cochlear canal is visible in both petrosals because the anterior part of the pars cochlearis is broken, although less severely in the right, than in the left petrosal (Figs 1D–G, 2, 3). Minute foramina for blood vessels and sinuses are visible on the interior surface of the cochlear canal (Figs 2F, 3C), which we interpret to be connected to the circum-promontorium sinus plexus (*sensu* Kermack *et al.* 1981) inside the bone covering the pars cochlearis (visible in the endocast, see endocast section below). We can trace this network of small vessels (Figs 2A; 7A, B, E, F). Additional small nutritive foramina connected to these small vessels are also visible on the endocranial surface of the petrosal (Fig. 2F).

The internal auditory meatus is well preserved in both petrosals. The primary foramen for the facial nerve (VII) to enter the internal auditory meatus can clearly be identified, and can be traced to the incomplete cavum supracochleare that houses the geniculate ganglion (Figs 2F, 3C, 4) (Rougier *et al.* 1992, 1996; Ruf *et al.* 2013). The foramen for the cochlear nerve (VIII), and laterally to that the foramen for the vestibular nerve (VIII), are

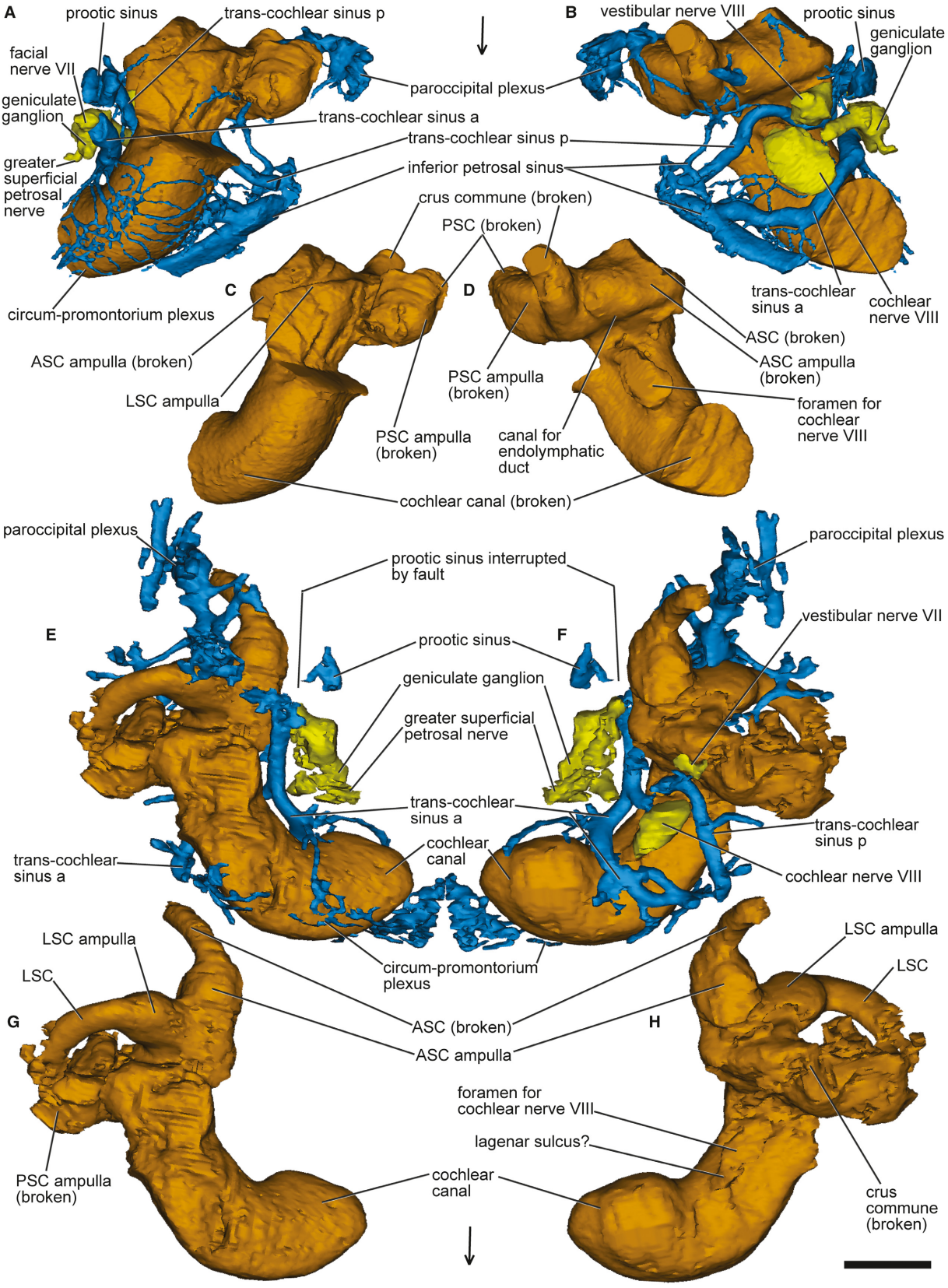
A
prootic sinus
trans-cochlear sinus p
facial nerve VII
geniculate ganglion
greater superficial petrosal nerve
paroccipital plexus
trans-cochlear sinus a
trans-cochlear sinus p
inferior petrosal sinus
crus commune (broken)
PSC (broken)
circum-promontorium plexus
B
vestibular nerve VIII
prootic sinus
geniculate ganglion
trans-cochlear sinus a
cochlear nerve VIII
C
ASC ampulla (broken)
LSC ampulla
PSC ampulla (broken)
D
ASC (broken)
ASC ampulla (broken)
PSC ampulla (broken)
foramen for cochlear nerve VIII
canal for endolymphatic duct
cochlear canal (broken)
paroccipital plexus
prootic sinus interrupted by fault
E
prootic sinus
geniculate ganglion
greater superficial petrosal nerve
trans-cochlear sinus a
cochlear canal
trans-cochlear sinus a
F
paroccipital plexus
vestibular nerve VII
trans-cochlear sinus p
cochlear nerve VIII
LSC ampulla
LSC
circum-promontorium plexus
G
ASC (broken)
ASC ampulla
PSC ampulla (broken)
H
LSC ampulla
LSC
foramen for cochlear nerve VIII
lagenar sulcus?
cochlear canal
crus commune (broken)

present. This structure is only partly preserved and can be clearly recognized in the left petrosal (NMS G.1992.47.121.2) (Fig. 2C–F). In the right petrosal (NMS G.1992.47.121.1), a fault-line has cut through this region, where the bone is also crushed laterally (Fig. 4, dashed line). The hollowed open space of the cavum supracochleare, as seen on the left, is crushed on the right petrosal. The large secondary facial nerve foramen is preserved in a similar position on both petrosals. This foramen is the exit of the facial nerve from the cavum supracochleare. On the left petrosal, the bone of the suprafacial commissure is broken, so the entire path of the facial nerve can be traced from the internal auditory meatus to the cavum supracochleare, and further from the cavum through to the secondary facial foramen.

In the left petrosal the prootic sinus groove continues as a prootic canal, perforating the petrosal just posterior to the cavum supracochleare. In the right petrosal, the bone in the area where the prootic groove would join the space of cavum supracochleare is distorted by crushing and displacement along the fault line that cuts through the prootic groove and the cavum supracochleare. As a result of this distortion, the relationship of these two structures is obscured in the right petrosal. Largely based on the location of the prootic canal opening on the external (tympanic) aspect of the left petrosal, we interpret the prootic sinus as traversing through the cavum supracochleare in a similar manner in the right petrosal (Wible & Hopson 1995). In the reconstructed dorsal-to-ventral sequence, the prootic sinus vein diverges from the sigmoid sinus at the top the subarcuate fossa. It then follows the prootic sinus groove along the lateral margin of the subarcuate fossa (Fig. 4), and enters the petrosal near the cavum epiptericum (Fig. 2). Inside the petrosal, the prootic sinus joins the lateral end of the posterior transcochlear sinus, before it enters the tympanic cavity through the prootic canal opening (Figs 2, 7A–B). Distally, the prootic sinus connects with the lateral head vein (Wible & Hopson 1995).

The cavum epiptericum, a bony space formed by the petrosal that houses the trigeminal ganglion of cranial nerve V, is preserved on the right petrosal (Figs 3, 4), but completely lost to damage on the left petrosal. Medially, the cavum epiptericum is separated from the internal auditory meatus by a saddle-shape structure known as the suprafacial commissure (Figs 3C, 4). Posteriorly, the cavum epiptericum is separated by a sliver of bone from the cavum supracochleare, but both the cavum epiptericum and the cavum supracochleare are in the same broader depression formed by the petrosal. This pattern is similar to features on the endocranial aspect of the petrosal in *Haldanodon* (Lillegraven & Krusat 1991) and *Morganucodon* (Kermack *et al.* 1981; Graybeal *et al.* 1989). This differs slightly from the petrosal of the Jurassic triconodontid *Priacodon*, in which the semilunar recess (related to the cavum epiptericum) is a large concave structure, in close proximity to the endocranial opening of the prootic canal (Rougier *et al.* 1996, fig. 1). The cavum supracochleare for the geniculate ganglion is present in *Priacodon*, but the bony floor of this space is interpreted as absent (Rougier *et al.* 1996, p. 9), a feature that also differs from the structure of *Borealestes* (Figs 3, 4).

The paroccipital region of the petrosal is relatively well preserved in the right petrosal, NMS G.1992.47.121.1 (Figs 5, 6). The anterior part of the paroccipital region is elevated from the rest of the petrosal. Its most notable structure is the Y-shaped crest of the crista parotica. We interpret the presence of a fossa incudis: a shallow depressed area accommodating the incus, which serves as the contact point of the incus and the petrosal. On the lateral side of the anterior paroccipital process, there is a broad depression representing part of the entoglenoid recess between the petrosal and the cranial moiety of the squamosal (Figs 5, 6). The posterior paroccipital process is excavated by a large and deep paroccipital pneumatic recess (*sensu* Ruf *et al.* 2013). The stylomastoid notch, which is the exit of the facial nerve from the tympanic region, is located medially to the base of the posterior paroccipital process (Fig. 6). The stapedial muscle fossa is a deep pit located posterior to the fenestra vestibuli and anteromedial to the posterior paroccipital process. The mastoid pneumatic recess is a deep excavation into the paroccipital-mastoid region of the petrosal, and is located medial to the stapedial muscle fossa and posterolateral to the perilymphatic foramen (Figs 5, 6). These petrosal structures of *Borealestes* are identical to those in the petrosal of the docodont *Haldanodon*, as described by Ruf

FIG. 7. Endocasts of interior structures of petrosals in *Borealestes*. A–D, left petrosal NMS G.1992.47.121.2: A, ventral view of the preserved inner ear endocast, with blood vessels and nerves; B, endocranial view the inner ear, with blood vessels and nerves; C, inner ear in ventral view (as preserved, incomplete), without vessels or nerves; D, inner ear in endocranial view (as preserved, incomplete) without vessels and nerves. E–H are of right petrosal NMS G.1992.47.121.1: E, ventral view of the preserved inner ear endocast, with blood vessels and nerves; F, endocranial view the inner ear, with blood vessels and nerves; G, inner ear in ventral view (as preserved, incomplete), without vessels or nerves; H, inner ear in endocranial view (as preserved, incomplete) without vessels and nerves. Blue = vascular structures, yellow = nerves. *Abbreviations*: a, anterior; ASC, anterior semi-circular canal; LSC, lateral semi-circular canal; p, posterior; PSC, posterior semi-circular canal. Arrows indicate anterior direction. All scale bars represent 1 mm.

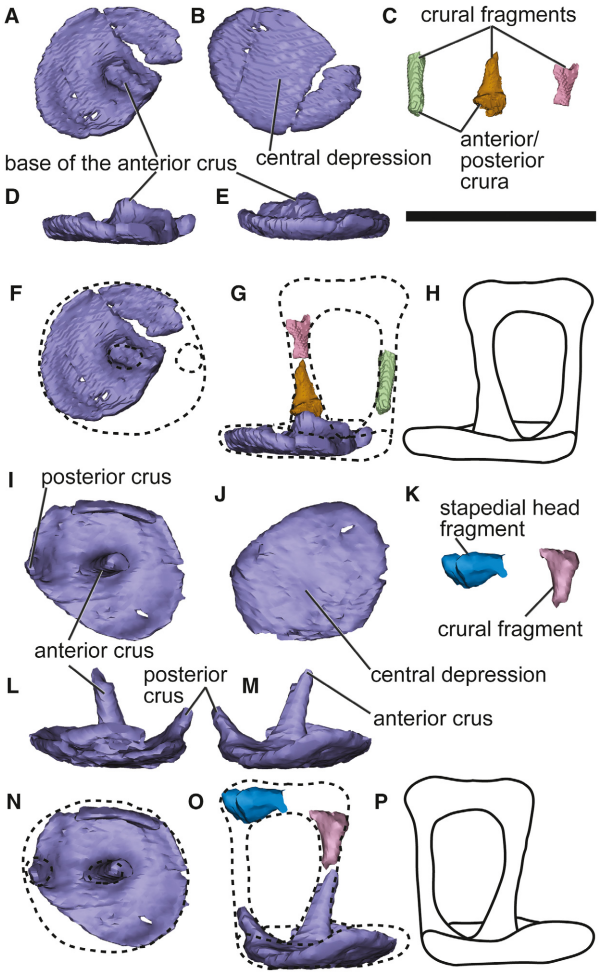

FIG. 8. Stapes of the docodont *Borealestes*. A–G, preserved parts of the left stapes NMS G.1992.47.121.2: A, left stapedial footplate (fractured and incomplete) in external view (from the inner ear space); B, left stapedial footplate (fractured and incomplete) in the internal view (toward the inner ear space); C, fragments of crura associated with the left stapedial footplate; D, approximately dorsal; and E, ventral side views of left stapedial footplate; F, interpretive reconstruction of external view of left stapedial footplate; G, interpretive reconstruction of crura from their fragments; H, interpretive reconstruction of side view of left stapes. I–O, preserved parts of the right stapes NMS G.1992.47.121.1: I, right stapedial footplate (incomplete) in external view (from the inner ear space); J, right stapedial plate (incomplete) in the internal view (toward the inner ear space); K, fragments of crura associated with the right stapedial footplate; L, approximately dorsal; and M, ventral side views of right stapedial footplate, showing the crural bases; N, interpretive reconstruction of the outline of right stapedial footplate in external view; O, interpretive association of crural fragments with their bases on footplate; P, interpretive reconstruction of side view of right stapes. All reconstructions based on remaining portions of stapes of NMS G.1992.47.121.1 and NMS G.1992.47.121.2, and the stapes of *Haldanodon* (Ruf *et al.* 2013). Scale bars represent 1 mm.

et al. (2013), with the four deeply excavated structures of the petrosal (paroccipital pneumatic recess, the stapedial fossa, the mastoid pneumatic recess, and the entoglenoid recess (partly on petrosal)) all strikingly similar between these two taxa.

The right petrosal (NMS G.1992.47.121.1) also preserves the bony channels and grooves for the arterial system from the superior ramus of the stapedial artery from the tympanic cavity and the arteria diploetica magna from the occiput (Wible 1990; Rougier *et al.* 1992; Wible & Hopson 1995). The pterygo-paroccipital foramen is located anterior to the crista parotica (Fig. 6). The foramen is represented by an open notch because the lateral border of this foramen is broken in this petrosal of *Borealestes*. By contrast, in the more complete petrosal of *Haldanodon*, the pterygoparoccipital foramen is fully encircled. This foramen is the passage for the superior ramus of the stapedial artery extant mammals and stem mammaliaforms (Wible 1990; Rougier *et al.* 1992; Wible & Hopson 1995). Dorsal of this foramen, the superior stapedial ramus follows an open groove lateral to the anterior paroccipital process and joins the arteria diploetica magna that enters through the post-temporal canal (partially preserved in right petrosal) (Fig. 6). The superior ramus of the stapedial artery and the arteria diploetica magna would be confluent with each other to form the ascending artery housed by the ascending vascular canal on the lateral side of petrosal that is also a part of the temporal skull surface. In the petrosal of *Haldanodon* (Lillegraven & Krusat 1991; Ruf *et al.* 2013) these structures are not fully exposed, or not fully segmented from the CT scans. The bony structures related to this vasculature, as revealed by CT scanning of the petrosal of *Borealestes*, are generally similar to those reconstructed for *Morganucodon*, and other Mesozoic mammals (Wible 1990; Rougier *et al.* 1992; Wible & Hopson 1995; Luo *et al.* 2012).

Endocast of the inner ear

Both petrosals were crushed post mortem, with the right petrosal being more complete. In both cases the inner ear endocasts are somewhat distorted. The approximate position of the fenestra vestibuli and perilymphatic foramen are identifiable despite this. Although the apex of the cochlear canal is absent in specimen NMS G.1992.47.121.2, it is clear that the canal is curved (Figs 2A–B, 7A–D), and this is confirmed by the more complete cochlear canal of the right petrosal (Figs 3A–B, 7E–H). The degree of curvature/coiling is similar to that of *Haldanodon* (Ruf *et al.* 2013), which can be traced in the right petrosal of *Borealestes*.

Vascular channels in pars cochlearis

The high quality of our scans (at a resolution of 12.3 and 8.9 μm) permits the reconstruction of some vascular channels and networks of small blood vessels in the bone of the pars cochlearis (Fig. 7). Some of these networks of tiny vessels can be directly traced and shown to be connected to the structures inside the bony labyrinth (Figs 2, 3A–B, 7). A noteworthy feature of these is the circum-promontorial sinus plexus (*sensu* Kermack *et al.* 1981) a network of tiny vessels (probably venous in nature) embedded in the pars cochlearis on the ventromedial side of the cochlear canal. This vascular network connects to the inferior petrosal sinus along the medial side of the promontorium (pars cochlearis) (Figs 2A, B; 3A, B; 7A, B, E, F). We also identify two relatively large vascular channels that traverse the bone of the pars cochlearis. We interpret these as probably venous in nature due to their full connections to other sinuses or veins (Figs 2, 3, 7). We have here termed these two major channels the anterior and posterior trans-cochlear sinuses (Figs 2, 3, 7).

The anterior trans-cochlear sinus (a) connects medially with the inferior petrosal sinus. From there it traverses through the bone of the pars cochlearis and enters laterally into the space of the cavum supracochleare (Figs 2, 3), the space that houses the geniculate ganglion of the facial nerve. Inside the pars cochlearis the course of anterior trans-cochlear sinus curves anteriorly around the bony internal auditory meatus. The opening for the secondary foramen of the facial nerve (VII) is very large in both left and right petrosals. This foramen could accommodate the passage of additional structure, such as the anterior trans-cochlear sinus. We therefore offer a speculative interpretation that the anterior trans-cochlear sinus exits through the enlarged secondary facial foramen, along with the facial nerve.

The posterior trans-cochlear sinus (p) starts in the posteromedial corner of the promontorium near the jugular notch, originating from a single large foramen in the left petrosal (Fig. 2), or in two foramina as in the right petrosal (Fig. 3). The bony course of this sinus is positioned more posteriorly than, and away from, the anterior trans-cochlear sinus. It curves around the main opening of the internal auditory meatus, and between the cochlear nerve foramen and the vestibular nerve foramen (Figs 2, 3, 7). The posterior trans-cochlear sinus is confluent with the prootic canal, suggesting that this sinus is connected to the prootic vein, before the prootic vein exits the petrosal into the tympanic region at the prootic canal opening (Fig. 2).

The anterior and posterior trans-cochlear sinuses are connected below the facial nerve geniculate ganglion in the cavum supracochleare, as shown in the right petrosal (Figs 3B, 7F). However, this confluence is not observed in the left petrosal, where anterior trans-cochlear sinus and posterior trans-cochlear sinus remain separate below the geniculate ganglion. This feature may be bilaterally variable, or the asymmetry may be an artefact of preservation.

We also recognize a network of small vessels in the paroccipital region of the petrosal, just underneath the entoglenoid recess. This corresponds to the squamosal plexus (Ruf *et al.* 2013, fig. 4). Altogether, these venous features demonstrate a high degree of vascularization of the cochlea and surrounding osteological structures of the pars cochlearis, as initially observed in *Haldanodon* (Ruf *et al.* 2013).

The internal auditory meatus on the endocranial aspect of the petrosals is relatively shallow, somewhat similar to that in the petrosal of *Morganucodon* (Kermack *et al.* 1981). The floor is divided by a low crest (crista falciformis) into a ventral depression for the large foramen of the cochlear nerve, and a dorsal depression for the primary facial nerve foramen and the foramen for the vestibular nerve (Figs 2F, 3C). The bony floor of the cochlear nerve foramen is preserved as a large and long slit in the right petrosal (Figs 1G, 3, 4) but this foramen appears to be broken widely open on the left petrosal (Fig. 2). The sulcus for the lagenar nerve as found in inner ear endocast in *Haldanodon* (Ruf *et al.* 2013, fig. 6) corresponds in position to part of the wide opening outline of the cochlear foramen in *Borealestes*. In the endocast of the right petrosal there is a suggestion of a possible lagenar nerve sulcus, but it cannot be conclusively identified in both petrosals of *Borealestes* due to lack of preservation.

Due to breakage of the anterior part of the pars cochlearis in the left petrosal (NMS G.1992.47.121.2), the anterior part of the internal auditory meatus that would encircle the primary facial nerve foramen is incomplete in this specimen. Fortuitously, this helps to expose the entrance of the facial nerve (VII) into the petrosal, and the facial nerve's conduit leading to the space for the geniculate ganglion can be clearly identified (Fig. 2F). In our digital reconstruction, the vestibular nerve (VIII) appears to be close to the primary facial nerve and the geniculate ganglion (Figs 7B). This is because the primary facial nerve foramen is in close proximity to the foramen of the vestibular nerve (Figs 2F, 3C), and both are situated together in dorsal depression in the floor of the internal auditory meatus. In the petrosals of other mammaliaforms described so far, the passages of the vestibular nerve (VIII) and the facial nerve (VII) are clearly more widely separated (Kermack *et al.* 1981; Graybeal *et al.* 1989; Ruf *et al.* 2013; also pers. obs. on *Sinoconodon* and *Hadrocodium*).

Stapes

Among the bone fragments displaced into the interior of both petrosals (Fig. 1H, I), we recovered parts of the left

and right stapes (Fig. 8). We identify a posterior and anterior stapedial crura, and crural fragments (Fig. 8). In the left petrosal, the stapedial footplate is fractured into three pieces which, we estimate, together constitute about 70% of the entire footplate (Fig. 8A–H). The reconstructed footplate has a nearly circular outline and is overall convex proximally toward the inner ear space. The lateral (external) aspect of the footplate is slightly concave, with curved edges around the periphery. The stapedial footplate recovered from the right petrosal (Fig. 8I–P) is more complete and confirms the position of the crura and the round shape of the footplate. The morphology of the bullate footplate resembles the stapes of *Haldanodon* (*sensu* Sánchez-Villagra & Nummela 2001; Ruf *et al.* 2013).

Both stapes show a central protruding bony knob preserved on the concave side (the lateral surface) of the footplate, which represents the base of the anterior crus (Fig. 8). We recovered additional separated pieces of bone that can be identified as fragments of the stapedial crura; the crural fragment coloured orange in Figure 8C (the middle fragment of the three) is most likely to be the lateral portion of the anterior crus. The two other fragments may be parts of the anterior or the posterior crus (Fig. 8G). The right stapes even has longer parts of each crus preserved in anatomical position, which indicate a square outline of the stapedial head (Fig. 8I–P). In addition, we interpret the rather bulbous fragment (Fig. 8K, blue coloured left-hand fragment) recovered from the right petrosal as part of the stapedial head (Fig. 8O). The stapedial footplate has a length of approximately 0.8 mm, and width of approximately 0.6–0.7 mm (based on measurements of both stapedial footplates), giving it a stapedial ratio of 0.75–0.86. However, the exact ratio is not certain due to the broken periphery of the footplate.

DISCUSSION

The petrosal and endocast of *Borealestes* is morphologically similar to that of *Haldanodon*, but there are some key differences that separate the two genera. A bony ridge visible on the anterolateral aspect (Figs 2E, 4A, 6) corresponds to a similar bony ridge in the same position on the petrosal of *Haldanodon* (Ruf *et al.* 2013). The anterior part of the cochlear canal is clearly curved, and the apical region of the curved cochlear canal is slightly inflated, as can be determined in the right petrosal of *Borealestes* (Fig. 7E–H). Both of these features on the right inner ear endocast are consistent with the incomplete inner ear endocast on the left side. The degree of curvature/coiling and apical inflation appears similar to that of *Haldanodon* (Ruf *et al.* 2013).

In *Haldanodon*, the anterior rim of the fenestra vestibuli is separated from the tympanic openings of the prootic canal, the secondary facial foramen, and from the hiatus Fallopii (Ruf *et al.* 2013, fig. 2). In the same region of petrosal of *Borealestes*, the fenestra vestibuli is also separated from these structures. However, *Borealestes* has an elevated crest in continuation with the bony ridge of the promontorium on the left petrosal (the same region is damaged on the right petrosal). This crest separates the fenestra vestibuli and the prootic canal opening (Fig. 2C, E). Such a crest is not present in *Haldanodon* and therefore *Borealestes* is different in this feature.

The morphology of the stapedial footplate is bullate as in *Haldanodon* (*sensu* Sánchez-Villagra & Nummela 2001; Ruf *et al.* 2013). In their description of the stapes of *Haldanodon exspectatus*, Ruf *et al.* (2013) reconstructed the stapes as having parallel anterior and posterior crus, with a large stapedial foramen. This is consistent with cynodonts and stem mammals for which the stapes is known (Novacek & Wyss 1986; Lillegraven & Krusat 1991; Allin & Hopson 1992; Crompton & Luo 1993; Luo 2007; Gaetano & Abdala 2015; Schultz *et al.* 2018). The stapedial footplates of *Haldanodon* and *Borealestes* are now almost equally well-known. In *Haldanodon*, the stapedial head is smaller than the stapedial footplate, the anterior crus is in central position, and the posterior crus is on the rim of the stapedial footplate. The rim of the stapedial footplate is slightly curved upward (bullate shape) and the stapedial footplate is basically round. Because *Borealestes* and *Haldanodon* are both docodonts, and phylogenetic analyses indicate they are closely related within a subclade of docodonts (Ji *et al.* 2006; Luo & Martin 2007; Averianov *et al.* 2010; Ruf *et al.* 2013; Luo *et al.* 2015*b*; Schultz *et al.* 2018), our reconstruction of the stapes of *Borealestes* (augmented by information from that of *Haldanodon*) is justifiable on a phylogenetic basis (Fig. 8H, P).

New key features identified in both petrosals of *Borealestes* are the two vascular sinuses that traverse the pars cochlearis: trans-cochlear canal anterior (a) and trans-cochlear canal posterior (p) (Figs 2A–B, 3A–B, 7). These connect to the large channels of the inferior petrosal sinus; the venous vessels extending in an anteroposterior direction along the medial side of the pars cochlearis of the petrosal. Within the bone of the pars cochlearis, the trans-cochlear canals are also connected to the circumpromontorium plexus. The inferior petrosal sinus is a major vascular structure in petrosals among Mesozoic groups of crown mammals (Rougier *et al.* 1992; Rougier *et al.* 1996; Luo *et al.* 2012; Hughes *et al.* 2015). For crown therians, this feature is well documented in Cretaceous and Paleocene metatherians (Wible 1990; Ladevèze & de Muizon 2007, 2010). In the petrosals of *Borealestes*, the channel for the inferior petrosal sinus, the circumpromontorium plexus, and the two trans-cochlear vascular sinuses (Figs 2A, B; 3A, B; 7A, B, E, F), form a well-developed vascular network. This corroborates earlier

observations that the petrosals of docodonts are highly vascularized, more so than that of *Morganucodon* (Kermack *et al.* 1981; Graybeal *et al.* 1989). In extant monotremes, the petrosal does not have the heavy vascularization in these regions, in contrast to *Haldanodon* and *Borealestes*' extensive vascularization throughout the petrosal (Kuhn & Zeller 1987; Ruf *et al.* 2013).

The trans-cochlear sinuses in the petrosal of *Borealestes* are newly recognized anatomical features. Either these are unique features (autapomorphic) of *Borealestes*, or they could be derived features (apomorphic) of docodonts as a whole if their presence can be confirmed by re-scanning and re-segmenting the petrosal of *Haldanodon*, or petrosals of other docodonts. These two sinuses are also interesting in their connection to other vessels. The posterior trans-cochlear sinus connects from the endocranial opening of the prootic (venous) sinus through the pars cochlearis to the inferior petrosal sinus. This suggests that in *Borealestes* the prootic sinus was connected to the inferior petrosal sinus. The posterior trans-cochlear sinus is confluent with the prootic sinus, and then exits through the prootic canal passing through the lateral trough of the petrosal (see Wible & Hopson 1995 and Rougier & Wible 2006 for overviews of the prootic canal in cynodonts). This vascular channel connection is a new finding and has not been previously documented in other mammaliaforms. However, the lack of these trans-cochlear sinuses in other mammaliaforms could be due to the fact that the interior structures in the petrosals of other mammaliaform have not yet been examined by such high-resolution μCT scanning as in our study of *Borealestes*.

The preserved features on the anterior and posterior paroccipital processes and in the mastoid region in the right petrosal of *Borealestes* (Figs 5, 6) are almost identical to the more complete homologues in *Haldanodon* (Ruf *et al.* 2013). The major excavated (presumably pneumatized) structures in these regions, and the degree of vascularization in the bone that form them, is similar in *Borealestes* and *Haldanodon* in the following: the entoglenoid recess (partly preserved); the well-developed paroccipital plexus; the prominent paroccipital pneumatic recess on the ventral aspect of the posterior paroccipital process; the depth of the stapedial muscle fossa; and the deep mastoid pneumatic recess. The pneumatization of the exterior surface structures in the paroccipital and mastoid regions of the petrosal, and high degree of vascularization in the bones forming these structures are unique and derived features of *Borealestes* and *Haldanodon*, and possibly of docodonts as a group.

The overall morphology of the inner ear of *Borealestes* is similar to that of *Haldanodon*, and implies similar hearing capabilities in these two genera of docodont. The vascularization in the petrosal of *Haldanodon*, the presence of a paroccipital pneumatic recess, and curvature of the cochlea were all considered to be evidence in support of a fossorial lifestyle in that genus by Ruf *et al.* (2013). This was coupled with features such as vascularization in the rest of the basicranium, and thicker lateral and posterior semi-circular canals (Ruf *et al.* 2013). As these additional features are not preserved in *Borealestes*, we can only tentatively infer a similar lifestyle for these two taxa. The hypothesis about a fossorial lifestyle of *Borealestes* can be tested when the postcranial morphology is more fully revealed; the petrosals described here are part of a larger morphological study of a nearly complete specimen of the *Borealestes* skeleton NMS G.1992.47.121.1 (currently under study by EP). The additional cranial material, coupled with postcranial elements, are expected to shed further light on the palaeobiology of *Borealestes* in the future.

CONCLUSIONS

The high-resolution of our computed tomography and synchrotron scans has enabled us to characterize the details of the vascularized structures of the petrosal of *Borealestes*, and provide the first endocranial view of a docodont petrosal. This has led to the identification of two previously unknown structures: the anterior and posterior trans-cochlear sinuses. This has also made it feasible for us to develop an overall reconstruction of the vascular and innervation structure in the petrosal. Despite post mortem crushing and the displacement of fragments of the petrosal and stapes inside the cochlear canal, we have been able to digitally reconstruct broken fragments of the petrosal and stapes. This reveals a more or less circular fenestra vestibuli and stapedial footplate, with a bullate morphology, as in *Haldanodon*. There are broad similarities in the morphology of the petrosal of *Borealestes* to that of *Haldanodon*, from which we tentatively suggest a similar ecology for these two docodonts. Further skeletal material currently under study will allow us to further explore the ecology of *Borealestes*, and add to our understanding of ecomorphologcal diversity in Docodonta.

Acknowledgements. We would like to thank I. Butler at the University of Edinburgh for his time and expertise acquiring μCT scan data, and Vincent Fernandez at the ESRF for acquiring and reconstructing our unusually challenging synchrotron data. EP was funded by NERC, grant number NE/L002558/1, and synchrotron scans were allocated by ESRF. JAS was funded by the DAAD during this study, project 57073880. Z-XL was supported by the Division of Biological Sciences of University of Chicago, and by the National Science Foundation during this study. We are also grateful to National Museums Scotland for easy access to their collections and equipment, and the advice and guidance given by S. Walsh and N. Fraser from the museum's Natural Sciences Department. Our thanks to Brian M. Davis and Eric G. Ekdale who commented on an earlier draft of the manuscript.

DATA ARCHIVING STATEMENT

Data for this study are available in the Dryad Digital Repository: https://doi.org/10.5061/dryad.07934k0

Editor. Hannah O'Regan

REFERENCES

ALLIN, E. F. and HOPSON, J. A. 1992. Evolution of the auditory system in Synapsida ("mammal-like reptiles" and primitive mammals) as seen in the fossil record. 587–614. *In* WEBSTER, D. B., FAY, R. R. and POPPER, A. N. (eds). *The evolutionary biology of hearing*. Springer, 859 pp.

ANDREWS, J. E. 1985. The sedimentary facies of a late Bathonian regressive episode: the Kilmaluag and Skidiburgh Formations of the Great Estuarine Group, Inner Hebrides, Scotland. *Journal of the Geological Society*, **142**, 1119–1137.

AVERIANOV, A. O. and LOPATIN, A. V. 2006. *Itatodon tatarinovi* (Tegotheriidae, Mammalia), a docodont from the Middle Jurassic of Western Siberia and phylogenetic analysis of Docodonta. *Paleontological Journal*, **40**, 668–677.

—— —— KRASNOLUTSKII, S. A. and IVANTSON, S. V. 2010. New docodontans from the Middle Jurassic of Siberia and reanalysis of Docodonta interrelationships. *Proceedings of the Zoological Institute RAS*, **314**, 121–148.

BRITISH GEOLOGICAL SURVEY 2011. *Stratigraphic framework for the Middle Jurassic strata of Great Britain and the adjoining continental shelf: research report RR/11/06*. British Geological Survey, Keyworth, Nottingham.

CLOSE, R. A., DAVIS, B. M., WALSH, S., WOLONIEWICZ, A. S., FRIEDMAN, M. and BENSON, R. B. J. 2016. A lower jaw of *Palaeoxonodon* from the Middle Jurassic of the Isle of Skye, Scotland, sheds new light on the diversity of British stem therians. *Palaeontology*, **59**, 155–169.

CROMPTON, A. W. and LUO, Z.-X. 1993. The relationships of the Liassic mammals Sinoconodon, *Morganucodon oehleri* and *Dinnetherium*. 30–44. *In* SZALAY, F. S., NOVACEK, M. J. and McKENNA, C. (eds). *Mammal phylogeny. Vol. 1: Mesozoic differentiation, multituberculates, monotremes, early Therians, and marsupials*. Springer, 242 pp.

DATTA, P. M. 2005. Earliest mammal with transversely expanded upper molar from the Late Triassic (Carnian) Tiki Formation, South Rewa Gondwana Basin, India. *Journal of Vertebrate Paleontology*, **25**, 200–207.

EVANS, S., BARRETT, P., HILTON, J., JONES, M., PARRISH, J. and RAYFIELD, E. 2005. The Middle Jurassic vertebrate assemblage of Skye, Scotland. *Journal of Vertebrate Paleontology*, **25**, 54A–55A.

GAETANO, L. C. and ABDALA, F. 2015. The stapes of gomphodont cynodonts: insights into the middle ear structure of non-mammaliaform cynodonts. *PLoS One*, **10**, e0131174.

GRAYBEAL, A., ROSOWSKI, J. J., KETEN, D. R. and CROMPTON, A. W. 1989. Inner-ear structure in *Morganucodon*, an early Jurassic mammal. *Zoological Journal of the Linnean Society*, **96**, 107–117.

HU, Y.-M., MENG, J. and CLARK, J. M. 2007. A new Late Jurassic docodont (Mammalia) from northeastern Xinjiang, China. *Vertebrata PalAsiatica*, **45**, 173–194.

HUGHES, E. M., WIBLE, J. R., SPAULDING, M. and LUO, Z.-X. 2015. Mammalian petrosal from the Upper Jurassic Morrison Formation of Fruita, Colorado. *Annals of Carnegie Museum*, **83**, 1–17.

JI, Q., LUO, Z.-X., YUAN, C.-X. and TABRUM, A. R. 2006. A swimming mammaliaform from the Middle Jurassic and ecomorphological diversification of early mammals. *Science*, **311**, 1123–1127.

KERMACK, K. A., MUSSETT, F. and RIGNEY, H. W. 1981. The skull of *Morganucodon*. *Zoological Journal of the Linnean Society*, **71**, 1–158.

—— LEE, A. J., LEES, P. M. and MUSSETT, F. 1987. A new docodont from the Forest Marble. *Zoological Journal of the Linnean Society*, **89**, 1–39.

KIELAN-JAWOROWSKA, Z., CIFELLI, R. L. and LUO, Z.-X. 2004. *Mammals from the age of dinosaurs: Origins evolution and structure*. Columbia University Press, 630 pp.

KRUSAT, G. 1980. Contribuçao para o conhecimento da fauna do Kimeridgiano da mina de lignito Guimarota (Leiria, Portugal). IV Parte. *Haldanodon exspectatus* Kuhne & Krusat 1972 (Mammalia, Docodonta). *Memorials dos Serviços Geologicos de Portugal*, **27**, 1–79.

KUHN, H. J. and ZELLER, U. 1987. The cavum epiptericum in monotremes and therian mammals. *Mammalia Depicta*, **13**, 51–70.

LADEVÈZE, S. and DE MUIZON, C. 2007. The auditory region of early Paleocene Pucadelphydae (Mammalia, Metatheria) from Tiupampa, Bolivia, with phylogenetic implications. *Palaeontology*, **50**, 1123–1154.

—— —— 2010. Evidence of early evolution of Australidelphia (Metatheria, Mammalia) in South America: phylogenetic relationships of the metatherians from the Late Palaeocene of Itaboraí (Brazil) based on teeth and petrosal bones. *Zoological Journal of the Linnean Society*, **159**, 746–784.

LILLEGRAVEN, J. A. and HAHN, G. 1993. Evolutionary analysis of the middle and inner ear of Late Jurassic multituberculates. *Journal of Mammalian Evolution*, **1**, 47–74.

—— and KRUSAT, G. 1991. Cranio-mandibular anatomy of *Haldanodon exspectatus* (Docodonta; Mammalia) from the Late Jurassic of Portugal and its implications to the evolution of mammalian characters. *Contributions to Geology, University of Wyoming*, **28**, 39–138.

LOPATIN, A. V. and AVERIANOV, A. O. 2005. A new docodont (Docodonta, Mammalia from the Middle Jurassic of Siberia. *Doklady Biological Sciences*, **405**, 434–436.

—— —— MASCHENKO, E. N. and LESCHCHINSKIY, S. V. 2009. Early Cretaceous mammals of Western Siberia: 2. Tegotheriidae. *Paleontological Journal*, **43**, 453–462.

LUO, Z.-X. 2001. Inner ear and its bony housing in tritylodonts and implications for evolution of mammalian ear. *Bulletin of Museum of Comparative Zoology*, **156**, 81–97.

—— 2007. Transformation and diversification in early mammal evolution. *Nature*, **450**, 1011–1019.

—— and MARTIN, T. 2007. Analysis of molar structure and phylogeny of docodontan genera. *Bulletin of Carnegie Museum of Natural History*, **39**, 27–47.

—— CROMPTON, A. W. and LUCAS, S. G. 1995. Evolutionary origins of the mammalian promontorium and cochlea. *Journal of Vertebrate Paleontology*, **15**, 113–121.

—— —— and SUN A.-L. 2001. A new mammaliaform from the Early Jurassic of China and evolution of mammalian characteristics. *Science*, **292**, 1535–1540.

—— KIELAN-JAWOROWSKA, Z. and CIFELLI, R. L. 2002. In quest for a phylogeny of Mesozoic mammals. *Acta Palaeontologica Polonica*, **47**, 1–78.

—— RUF, I. and MARTIN, T. 2012. The petrosal and inner ear of the Late Jurassic cladotherian mammal *Dryolestes leiriensis* and implications for ear evolution in therian mammals. *Zoological Journal of the Linnean Society*, **166**, 433–463.

—— —— SCHULTZ, J. A. and MARTIN, T. 2011. Fossil evidence on the evolution of inner ear cochlea in Jurassic mammals. *Proceedings of the Royal Society B*, **278**, 28–34.

—— GATESAY, S. M., JENKINS, F. A., AMARAL, A. A. and SHUBIN, N. H. 2015*a*. Mandibular and dental characteristics of Late Triassic mammaliaform *Haramiyavia* and their ramifications for basal mammal evolution. *Proceedings of the National Academy of Sciences*, **112**, E7101–E7109.

—— MENG, Q.-J., JI, Q., LIU, D., ZHANG, Y.-G. and NEANDER, A. I. 2015*b*. Evolutionary development in basal mammaliaforms as revealed by a docodontan. *Science*, **347**, 760–764.

—— SCHULTZ, J. A. and EKDALE, E. G. 2016. Evolution of the middle and inner ears of mammaliaforms: the approach to mammals. 139–174. *In* CLACK, J. A., FAY, R. R. and POPPER, A. N. (eds). *Evolution of the vertebrate ear*. Springer International Publishing, 355 pp.

MARTIN, T. 2005. Postcranial anatomy of *Haldanodon exspectatus* (Mammalia, Docodonta) from the Late Jurassic (Kimmeridgian) of Portugal and its bearing for mammalian evolution. *Zoological Journal of the Linnean Society*, **145**, 219–248.

—— AVERIANOV, A. O. and PFRETZSCHNER, H.-U. 2010. Mammals from the Late Jurassic Qigu Formation in the Southern Junggar Basin, Xinjiang, Northwest China. *Palaeobiodiversity & Palaeoenvironment*, **90**, 295–319.

MASCHENKO, E. N., LOPATIN, A. V. and VORONKEVICH, A. V. 2002. A new genus if tegotherid docodonts (Docodonta, Tegotheriidae) from the Early Cretaceous of West Siberia. *Russian Journal of Theriology*, **1**, 75–81.

MENG, Q.-J., JI, Q., ZHANG, Y.-G., LIU, D., GROSSNICKLE, D. M. and LUO, Z.-X. 2015. An arboreal docodont from the Jurassic and mammaliaform ecological diversification. *Science*, **347**, 764–768.

NOVACEK, M. J. and WYSS, J. 1986. Origin and transformation of the mammalian stapes. *Contributions to Geology, University of Wyoming, Special Paper*, **3**, 35–53.

PANCIROLI, E., BENSON, R. B. J. and WALSH, S. 2017*a*. The dentary of *Wareolestes rex* (Megazostrodontidae): a new specimen from Scotland and implications for morganucodontan tooth replacement. *Papers in Palaeontology*, **3**, 373–386.

—— WALSH, S., FRASER, N., BRUSATTE, S. L. and CORFE, I. 2017*b*. A reassessment of the postcanine dentition and systematics of the tritylodontid *Stereognathus* (Cynodontia, Tritylodontidae, Mammaliamorpha), from the Middle Jurassic of the UK. *Journal of Vertebrate Paleontology*, **37**, e1351448.

—— LUO, Z.-X. and SCHULTZ, J. A. 2018. Data from: Morphology of the petrosal and stapes of *Borealestes* (Mammaliaformes, Docodonta) from the Middle Jurassic of Skye, Scotland. *Dryad Digital Repository*. https://doi.org/10.5061/dryad.07934k0

PFRETZSCHNER, H.-U., MARTIN, T., MAISCH, M., MATZE, A. and SUN, G. 2005. A new docodont from the Late Jurassic of the Junggar Basin of northwest China. *Acta Palaeontologica Polonica*, **50**, 799–808.

PRASAD, G. V. R. and MANHAS, B. K. 2001. First docodont mammals of Laurasian affinities from India. *Current Science*, **81**, 1235–1238.

—— —— 2007. A new docodont mammal from the Jurassic Kota Formation of India. *Palaeontologia Electronica*, **10**, 7A.

ROUGIER, G. W. and WIBLE, J. R. 2006. Major changes in the ear region and basicranium of early mammals. 269–311. *In* CARRANO, M. T., GAUDIN, T. J., BLOB, R. W. and WIBLE, J. R. (eds). *Amniote paleobiology: Phylogenetic and functional perspectives on the evolution of mammals, birds, and reptiles*. University of Chicago Press, 448 pp.

—— —— and HOPSON J. A. 1992. Reconstruction of the cranial vessels in the Early Cretaceous mammal *Vincelestes neuquenianus*: implications for the evolution of the mammalian cranial vascular system. *Journal of Vertebrate Paleontology*, **12**, 188–216.

—— —— —— 1996. Basicranial anatomy of *Priacodon fruitaensis* (Triconodontidae Mammalia) from the Late Jurassic of Colorado, and a reappraisal of mammaliaform interrelationships. *American Museum Novitates*, **3183**, 1–38.

—— SHETH, A. S., CARPENTER, K., APPELLA-GUISDAFRE, L. and DAVIS, B. M. 2015. A new species of *Docodon* (Mammaliaformes, Docodonta) from the Upper Jurassic Morrison Formation and a reassessment of selected craniodental characters in basal mammaliaforms. *Journal of Mammalian Evolution*, **22**, 1–16.

RUF, I., LUO, Z.-X., WIBLE, J. R. and MARTIN, T. 2009. Petrosal anatomy and inner ear structures of the Late Jurassic *Henkelotherium* (Mammalia, Cladotheria, Dryolestoidea): insight into the early evolution of the ear region in cladotherian mammal. *Journal of Anatomy*, **214**, 679–693.

—— —— and MARTIN T. 2013. Reinvestigation of the basicranium of *Haldanodon exspectatus* (Mammaliaformes, Docodonta). *Journal of Vertebrate Paleontology*, **33**, 382–400.

SÁNCHEZ-VILLAGRA, M. R. and NUMMELA, S. 2001. Bullate stapes in some phalangeriform marsupials. *Mammalian Biology*, **66**, 174–177.

SCHULTZ, J. A., BHULLAR, B. A. S. and LUO, Z.-X. 2017*a*. Re-examination of the Jurassic mammaliaform *Docodon victor* by computed tomography and occlusal functional

analysis. *Journal of Mammalian Evolution*, published online 15 December. https://doi.org/10.1007/s10914-017-9418

—— ZELLER, U. and LUO, Z.-X. 2017*b*. Inner ear labyrinth anatomy of monotremes and implications for mammalian inner ear evolution. *Journal of Morphology*, **278**, 236–263.

—— RUF, I. and MARTIN, T. 2018. Oldest known multituberculate stapes suggests an asymmetric bicrural pattern as ancestral for Multituberculata. *Proceedings of the Royal Society B*, **285**, 20172779. https://doi.org/10.1098/rspb.2017.2779

SIGOGNEAU-RUSSELL, D. 2003. Docodonts from the British Mesozoic. *Acta Palaeontologica Polonica*, **48**, 357–374.

—— and HAHN, R. 1995. Reassessment of the Late Triassic symmetrodont mammal *Woutersia*. *Acta Palaeontologica Polonica*, **40**, 245–260.

SIMPSON, G. G. 1929. American Mesozoic Mammalia. *Memoirs of the Peabody Museum of Yale University*, **3**, 1–235.

WALDMAN, M. and SAVAGE, R. J. G. 1972. The first Jurassic mammal from Scotland. *Journal of the Geological Society of London*, **128**, 119–125.

WIBLE, J. R. 1990. Petrosals of Late Cretaceous marsupials from North America and a cladistics analysis of the petrosal in therian mammals. *Journal Vertebrate Paleontology*, **10**, 183–205.

—— and HOPSON, J. A. 1993. Basicranial evidence for early mammal phylogeny. 45–62. *In* SZALAY, F. S., NOVACEK, M. J. and McKENNA, C. (eds). *Mammal phylogeny. Vol. 1: Mesozoic differentiation, multituberculates, monotremes, Early Therians, and marsupials*. Springer, 242 pp.

—— —— 1995. The homologies of the prootic canal in mammals and non-mammalian cynodonts. *Journal of Vertebrate Paleontology*, **15**, 331–356.